

The Abundance of Interstellar Fluorine and Its Implications

Theodore P. Snow, Joshua D. Destree, and Adam G. Jensen

Center for Astrophysics and Space Astronomy

Department of Astrophysical and Planetary Sciences, University of Colorado at Boulder

Campus Box 389

Boulder, CO 80309-0389

tsnow@casa.colorado.edu, destree@casa.colorado.edu, Adam.Jensen@colorado.edu

ABSTRACT

We report results from a survey of neutral fluorine (F I) in the interstellar medium. Data from the *Far Ultraviolet Spectroscopic Explorer (FUSE)* were used to analyze 26 lines of sight lying both in the galactic disk and halo, including lines to Wolf-Rayet stars and through known supernova remnants. The equivalent widths of fluorine resonance lines at 951.871 Å and 954.827 Å were measured or assigned upper limits and combined with a nitrogen curve of growth to obtain F I column densities. These column densities were then used to calculate fluorine depletions. Comparisons are made to the previous study of F I by Federman et al. (2005) and implications for F I formation and depletion are discussed.

1. Introduction: Fluorine in the interstellar medium

Fluorine (element 9, with only one stable isotope [^{19}F]) is the most reactive species observed in the diffuse interstellar medium. The diatomic molecule HF is predicted to be abundant, as it is formed by an exothermic neutral-neutral reaction of atomic fluorine (F I) with H_2 . The abundance of HF should compete with, or even dominate over, the abundance of F I in molecular clouds, despite the slow reaction rate of F I with H_2 (Zhu et al. 2002). In such dense clouds, F I also can be converted rapidly into CF^+ (Neufeld, Wolfire, & Schilke 2005). But in diffuse molecular clouds (i.e., regions where some of the hydrogen, but not all, is in molecular form; see Snow & McCall 2006), HF should still be detectable but not dominant over F I. In these clouds, F I is observed in the gas phase, as demonstrated previously by Snow and York (1981) and Federman et al. (2005).

There are three possible formation mechanisms for fluorine: (1) Type II supernovae, through a neutrino capture process starting from ^{20}Ne , typically called the ν -process (Woosley & Haxton, 1988 and Woosley & Weaver, 1995), (2) Wolf-Rayet stars, through internal helium burning followed by rapid ejection in stellar winds (Meynet & Arnould, 2000), and (3) in asymptotic giant branch (AGB) stars, again through helium burning followed by mass loss (Forestini et al. 1992). In all three scenarios rapid mass loss is required, as fluorine is destroyed in thermodynamic equilibrium almost as soon as it forms, through α -captures leading to ^{16}O and ^{22}Ne . Thus the galactic abundance of fluorine might help to distinguish among the possible formation mechanisms, which in turn can improve our understanding of the nucleosynthesis history of the Sun and other stars. However, for various reasons, this element has not been widely observed in its atomic form despite its implications for the history of nucleosynthesis in the Galaxy.

Some observational evidence regarding fluorine formation, especially concerning AGB stars, has been reported since the various formation mechanisms were proposed. Though some of the findings seem to conflict, most support AGB stars as a fluorine production site. Jorissen, Smith and Lambert (1992) used rotation-vibration lines of HF to obtain fluorine abundances in red giants. They found an overabundance of fluorine in C-rich stars, indicating that fluorine could indeed be produced in AGB stars. Similarly, Cunha et al. (2003) used HF rotation-vibration lines to study fluorine in the Large Magellanic Cloud and ω Centauri. In general, ω Centauri is largely enriched in elements formed through the s-process in AGB stars. This study, however, found low F/O ratios in two ω Centauri stars with low metallicities, indicating that fluorine was not enriched along with the s-process elements in the cluster. Thus, it was concluded that AGB stars do not play a dominant role in the formation of fluorine. Soon after, though, more evidence for fluorine formation in AGB stars was reported by Werner, Rauch, and Kruk (2005), as they detected great fluorine overabundances using absorption lines from highly ionized fluorine in *Far Ultraviolet Spectroscopic Explorer* (*FUSE*) spectra. Recently, Federman et al. (2005) studied fluorine in the ISM towards two stars in the Cep OB2 association using the 954 Å F I line in *FUSE* data. They found no indication of fluorine enhancement resulting from Type II supernovae. A study by Zhang and Liu (2005) observed emission lines in a sample of planetary nebulae and found fluorine to be generally overabundant, providing more evidence for AGB stars playing an important role in fluorine nucleosynthesis. Additionally, they saw a large fluorine enhancement in NGC 40, a planetary nebula whose central star is a Wolf-Rayet star, suggesting that rapid mass loss as seen in Wolf-Rayet stars favor fluorine formation.

Improved modeling of these formation mechanisms can also help answer the questions behind fluorine nucleosynthesis. A recent model by Renda et al. (2005) takes into account fluorine production from all three possible sources. They find that a model Milky Way

including all three fluorine production mechanisms most closely matches the current observed fluorine abundances.

In this study we use *FUSE* far-ultraviolet spectra to determine the interstellar F I abundances in several lines of sight, with the hope of helping to constrain the origin of fluorine in the universe. The abundance of fluorine in the diffuse ISM can be measured through its pair of ground-state atomic F I absorption lines in the far-ultraviolet, at wavelengths of 951.871 Å and 954.827 Å (though usually only the 954 Å line is detected). In dense clouds, some transitions of fluorine-based compounds can be observed as well (Neufeld, Wolfire, & Schilke, 2005). The HF molecule was observed in the ISM using the $J = 2-1$ rotational line by Neufeld et al. (1997) and CF^+ was just recently discovered by Neufeld et al. (2006) toward the Orion Bar region through emission from three rotational transitions.

In this paper we present the results of a *FUSE*-based survey of F I column densities in a sample of 26 moderately reddened stars, selected for maximum gas column density observable below the threshold where the F I features become totally obscured by molecular hydrogen absorption. Our sample stars have E_{B-V} values ranging from 0.17 mag to 0.62 mag and total hydrogen column densities in the range from 0.4 to $3.2 \times 10^{21} \text{ cm}^{-2}$. This is the most extensive study of fluorine in diffuse interstellar clouds yet attempted.

The first detection of interstellar F I was reported by Snow and York (1981) on the basis of *Copernicus* spectra of δ Scorpii, but thereafter no one took up the pursuit until the recent *FUSE*-based study by Federman et al. (2005). Federman et al. observed the 954 Å line of F I in two stars in the Cepheus OB2 association and found evidence of slight ($\sim 45\%$) fluorine depletion relative to the abundance of this element in the Sun and in meteorites. Data on both can be found in Anders & Grevesse, 1989; Lodders, 2003; and Asplund, Grevesse, & Sauval, 2005 — all of which agree on the solar fluorine abundance to within ± 0.1 dex. Federman et al. provide extensive discussion of the nucleosynthetic implications of the interstellar fluorine abundance, which will not be repeated here except for comments in our discussion section.

In the following we present a description of the *FUSE* data and the rationale for our choice of targets from the archive (§2), a description of our methods for analyzing the data (§3), and a discussion of the results and their implications (§4).

2. Observations and Data Reduction

The *FUSE* mission continues to be a vital tool for analyzing the processes in interstellar clouds. This is largely due to the fact that several of the most abundant elements in

space have their ground-state transitions in the far ultraviolet, a wavelength region covered uniquely by *FUSE* but not by other ultraviolet (UV) instruments such as the *Hubble Space Telescope* (*HST*). *FUSE* is also more sensitive in throughput and/or spectral resolving power than previous instruments operated in the same wavelength interval, such as *Copernicus* or *ORFEUS*.

Stars in this study of fluorine were selected from the *FUSE* archive primarily from programs P101 and P102. We selected targets based on their ratios of signal to noise and on the existence of sufficient flux in the region immediately surrounding the 954 Å F I line. Table 1 shows the properties of all the analyzed lines of sight.

For all lines of sight, raw data were downloaded and processed with version 2.4.0 of the CALFUSE pipeline. All the observations were broken down into multiple exposures; so a cross-correlation analysis was performed on all detector segments before combining the spectra.

3. Data Analysis

In order to convert the observed F I absorption line strengths into column densities, the following steps were taken: (1) we removed the influence of molecular hydrogen absorption bands which partially overlie the F I lines, then (2) we developed a suitable curve of growth to take into account possible saturation of the F I lines. The first of these steps required us to model and remove the H₂ absorption; the second required us to develop a rationale for deducing the curve of growth that is most applicable to the F I lines.

3.1. H₂ Modeling

For nearly every target, molecular hydrogen lines of the $J = 0$ and $J = 1$ rotational states interfere with the region surrounding the 954 Å F I line. Thus, in order to determine the continuum and to measure the equivalent width of the fluorine line, we had to correct for the obstruction from H₂. This was done by creating a model of the molecular hydrogen absorption lines for the $J = 0, 1,$ and 2 rotational states. For lines of sight where a H₂ curve of growth analysis had already been performed, we took column densities from the literature, primarily Shull et al. (in preparation), for our sample.

For targets that had no available H₂ data, column densities were derived by fitting the 4-0 (1046-1054 Å), 2-0 (1075-1082 Å), and 1-0 (1091-1097 Å) Lyman bands of the spectrum in the LiF1A, LiF2A, and LiF2B segments. We first divided out any absorption features in

the region around the Lyman bands that were not H₂ lines of J = 0, 1, or 2 by fitting any obvious absorption features with a single Gaussian curve and then dividing the spectrum flux by that curve. A profile-fitting procedure was then used to derive the H₂ column densities. For details on this procedure see Rachford et al. (2002). Because a curve of growth analysis was not performed for H₂, we did not derive a *b*-value but used a value of $b = 5 \text{ km s}^{-1}$ for making the models. We can make this assumption because the J = 0 and 1 lines are usually heavily damped and thus are not sensitive to fine velocity structure or *b*-value. The J = 2 line is affected by our choice in *b*-value. However, since this line is not critical in our analysis and is only used for aligning the spectra, the value is not important. Derived H₂ column densities can be found in Table 2.

For HD 208440 and HD 209339 our H₂ column densities and those from Federman et al. (2005) generally agree within the 1- σ errors. The one discrepancy is the J = 2 column densities for HD 209339 which agree within 3- σ . This could be due in part to the very small error bars on the Federman et al. measurements. Error in H₂ column density for our study is the standard deviation of the individual fits of the three Lyman bands. This discrepancy in the J = 2 column density, though, does not in any way affect our analysis of F I because, as stated before, the J = 2 line is only used for aligning the model with our spectra.

Once we had a model of the molecular hydrogen, we performed a cross-correlation analysis on the region around the F I line to align the model and spectrum (see Figure 1). The H₂ model was correlated with the *FUSE* spectrum in the 954 Å to 957 Å region, relying heavily on the 956 Å J = 2 hydrogen line. Once aligned, the spectrum and corresponding error were divided by the hydrogen model to restore the continuum around the F I line.

3.2. Line Velocities

In assessing the F I line, whether present or absent, we needed to know where to look for it, which depends on the line of sight velocity structure. This is not a simple question because there are noticeable shifts between the atomic nitrogen (N I) and H₂ absorption lines in many cases. We expect the distribution of atomic fluorine to correlate to that of nitrogen because of the similarities in the two elements' ionization potentials. Thus, we are able to determine the expected F I line center based on nearby nitrogen features.

To confirm our assumption that F I and N I should arise at the same velocity, we also checked the atomic oxygen (O I) velocity in the two sight lines where N I and H₂ have very different velocities. We used O I as confirmation because, like fluorine, the ionization potential of oxygen is close to that of nitrogen. In both cases we found that the O I lines

were shifted the same amount from H₂ as the N I lines were. Thus, we felt confident that similar shifts for F I exist.

3.3. F I Equivalent Width Measurements

Once the spectrum was corrected, we obtained an equivalent width for both the F I lines by performing simple single Gaussian fits with second-order polynomials to fit the nearby continua (see Figure 2). In cases where the equivalent width for a F I lines was not significant to two standard deviations, we give a 2σ upper limit. Measured equivalent widths, upper limits, and errors are presented in Table 3.

3.4. N I Curve of Growth

Since we had only one F I line in most cases, we could not derive an empirical curve of growth from F I alone. Instead, based on the similarities between the expected distribution of N I and F I in space, we have assumed that the curve of growth for F I will be very similar to that for N I.

To find a curve of growth for N I, we measured the equivalent widths for as many N I absorption lines as possible within the range of the *FUSE* spectrum. We then fit all these measured lines to a curve of growth to find the column density and b -value for N I, assuming a single velocity component (see Figures 3, 4, 5, 6, and 7). Where data were available, we checked our assumption of a single velocity component by observing the 1356 Å O I line in *HST* STIS spectra. For most of the lines of sight that had *HST* data, we found only a single velocity component. Two sightlines (HD 37367 and HD 93250) showed two or more clearly separated velocity components. However, we find that in these cases the N I curves of growth are still internally consistent. Furthermore, the broad separation of the components of the 1356 Å O I line indicates that the total profiles of lines in *FUSE* data should still be optically thin as long as each component is optically thin. Again, this is supported by the internal consistency of the curves of growth, even when a large b -value is implied. The F I lines under examination are approximately as weak as or weaker than the weakest N I lines used in the curves of growth, and the use of the derived N I b -values to place limits on saturation is therefore justified. N I column densities and b -values are given in Table 4. For more details on the procedure used for deriving the N I curve of growth see Jensen, Rachford, & Snow, (2006).

3.5. Fluorine Column Densities

Once a curve of growth was established for N I, we used this same curve to find the column densities for F I from our measured equivalent widths. Errors in column densities were derived by carrying through the one-sigma errors on the Gaussian fit of the F I line. Errors in the curve of growth itself are not significant because the F I lines are weak enough in most cases to be on the linear part of the curve. In cases where we could not obtain a significant measurement of the fluorine equivalent width, we calculated a 2σ upper limit for the column density. Final fluorine column densities and limits are given in Table 5.

3.6. Comparison to Previous Work

The only other studies deriving interstellar F I column densities were done by Snow and York (1981) and by Federman et al. (2005).

Snow and York, using data from the *Copernicus* satellite, detected the 954 Å F I line toward δ Scorpii, and derived an F/H ratio based on the assumption that the F I line was weak enough to be on the linear portion of the curve of growth. They found an F I column density of $13.18_{-0.14}^{+0.15}$.

The Federman et al. study based on *FUSE* spectra analyzed two lines of sight, which we have also included in our survey: HD 208440 and HD 209339. A comparison of results can be found in Table 6. We find that our results match those from the Federman et al. study almost exactly, well within the $1\text{-}\sigma$ errors.

3.7. The 951 Å Line of F I

The secondary line of F I lies at 951.871 Å, which is also accessible to *FUSE*. The f-value of this line is weaker by a factor of five than the f-value of the 954 Å line, but in some cases might be detectable. We may have detected the line in five cases. Where we did not detect it, the upper limit helped us to constrain the curve of growth independent of the N I analysis.

The sightlines where we may have detected the 951 Å F I line are HD 37367, HD 103779, HD 164816, HD 165052, and HD 191877. Plots of both the suspected 951 Å and 954 Å lines for these stars are given in Figures 8 and 9.

For HD 103779, HD 164816, HD 165052, and HD 191877 both F I lines were measured with a single Gaussian to at least two-sigma significance. So for each of these cases we derived

a curve of growth based solely on the two F I lines (see Figure 10). From these curves we calculated F I column densities and b -values and compared them to those acquired using the N I curve of growth (See Table 7). The values derived from these two methods agree with one another. Since we only have two points on the curve, we cannot perfectly constrain its shape, so errors in derived column densities and b -values are obtained by letting each variable in turn change while the other is held at its derived optimal value.

HD 37367 had a strong absorption feature at the wavelength of the 951 Å F I line (Figure 8), and the wavelength shift of this line matched the shifts of nearby N I lines. However, this line of sight had very little flux in the region around the 954 Å F I line, making the 954 Å line immeasurable. Additionally, HD 37367 has a low $v \sin(i)$ value (~ 20 km/s) making stellar lines narrow and not easily distinguishable from interstellar features. Thus, for this sightline we calculated the column density based on the 951 Å feature, but because the spectra are so confusing, we cannot confidently say that the feature at 951 Å is F I, especially without the detection of the 954 Å feature.

One sightline through the Monoceros Loop supernova remnant (HD 47240) appeared to have a very strong absorption feature at the wavelength of the 951 Å F I line. An analysis of the velocity structure for this line of sight revealed this feature to most likely be a high velocity (~ 70 km/s) component of the nearby H₂ J = 3 line.

In our final analysis of F I column densities, we took the detections, or upper limits, on the F I 951 Å line into account, which helped us to refine our errors and improve our confidence in the F I column densities.

3.8. Discrepancies when Measuring the 954 Å Line of F I

In two lines of sight, HD 93205 and HD 103779, it is unclear whether the line at 954 Å is F I or not. In the spectrum of HD 93205, there is a large absorption feature at the wavelength of the 954 Å F I line; however, we do not believe this feature to be F I but rather a high velocity (~ -90 km/s) component of the nearby H₂ J = 1 line. Thus, for HD 93205 we have not claimed a detection of F I but only assign a 2σ upper limit. For HD 103779 the absorption feature at 954 Å is wider than in other lines of sight. This is not surprising, though, as we find the N I b -value to be high (17.3 km/s) and high resolution observations show two or more components spanning about 30 km/s in velocity space (Jenkins, & Tripp, 2001).

As mentioned earlier, we expect F I to be similarly distributed in space as N I and we nearly always observe F I wavelength shifts to indeed match those of N I. However, in three

cases (HD 164816, HD 165052, and HD 315021) both F I lines’ central wavelengths do not seem to correlate to those of N I. Interestingly, all three of these stars are located in NGC 6530, a young cluster and star forming region in the Lagoon Nebula (M 8). In two of these lines of sight (HD 164816 and HD 165052) we were able to measure both the 954 Å and 951 Å F I lines, making us confident that we are indeed measuring F I. The appearance of the same shift in three different lines of sight confirms that this is not just coincidental to one line of sight but that the effect is real. However, we are unable at this point to explain why F I would not have the same velocity structure as N I in these lines of sight.

3.9. Fluorine Formation

As mentioned in the introduction, one of the main objectives in our study of fluorine is to determine what mechanisms are primarily responsible for the element’s formation. Thus we attempted to explore this topic by investigating Wolf-Rayet stars and sight lines that pass through known supernova remnants. Unfortunately this did not shed much light on any of the possible formation mechanism because of poor data quality and unidentified, interfering absorption features. For those lines of sight that did have sufficient flux, we set upper limits on the equivalent width of the 954 Å and 951 Å F I lines and derived upper limits on the F I column densities. Results can be found in Tables 3, 4, 5, and 8.

4. Discussion

We have detected F I absorption in 13 of our 26 targets, and provide upper limits for the remaining twelve, with HD 37367 ambiguous because of possible interference from narrow stellar features. Our range of reddening and total gas column density is restricted on both sides - at the lower limit by the minimum column density needed for the F I line to be detected, and on the upper side by the beginning of total obscuration of the F I line by molecular hydrogen absorption. Thus we are unable to explore fluorine depletions over a very wide range of cloud physical conditions. Any future studies will suffer the same limitations.

Nevertheless we can reach some useful conclusions about the fluorine abundances and depletions in the diffuse sightlines that we were able to probe. First, in general agreement with the results of Snow and York (1981) and of Federman et al. (2005) we find that fluorine is only slightly depleted, if at all, relative to the solar value for all of the sightlines where we obtained detections of F I absorption. Our values for depletion (Table 5) show F/H ratios ranging from about 0.1 to -0.6 dex.

Second, we do not see any sign of fluorine enhancement even in sightlines toward early O stars where the internal nucleosynthesis might have been expected to produce excess fluorine which was then expelled into the ISM through rapid stellar winds (i.e., the Wolf-Rayet mechanism mentioned in Section I). It is impossible to obtain UV spectra toward AGB stars, so the best way to determine fluorine abundances in those environments is either through the $J = 1-0$ HF absorption at $243 \mu\text{m}$, something that will become possible when the SOFIA aircraft is in operation (see discussion in Neufeld et al. 2005) or through the $J = 2-1$ HF absorption at $121 \mu\text{m}$ (Neufeld et al. 1997).

One possible explanation, though an unlikely one, for the lack of observed fluorine enhancement in early O stars could be that extra fluorine expelled from these stars is depleted rapidly into molecules or dust grains. If this were happening, it might explain why we do not see significant levels of either fluorine depletion or enhancement.

The slight depletion of atomic fluorine requires two conditions: (1) not much of the fluorine in the diffuse ISM is in molecular form; and (2) there is little depletion of fluorine onto dust grains. These points are apparently in disagreement with the predictions of Neufeld et al. (2005), if they were applied to dense clouds.

The hydride of fluorine, HF, is expected to compete with, or perhaps exceed, the abundance of atomic fluorine, depending on how abundant H_2 is. For molecular fractions approaching unity, HF should dominate over F I (Neufeld, Wolfire, and Schilke, 2005), but for H I regions, atomic fluorine should be dominant. Our H_2 fractions are in range from 0.1 to 0.4, so we should expect more F I than HF, which we see (we know that, because F I is nearly solar, as alluded to above and as described below). HF has been detected in emission toward the far-IR continuum source Sg2 B2 (at $121 \mu\text{m}$; Neufeld et al. 1997), but the far-UV line near 951 \AA has not been seen, though there are hints that it may be contributing to an overlapping N I line (Sonnentrucker and Neufeld, private communication).

Neufeld et al. (2005, 2006) stress that the abundance of HF is likely to peak just where the ambient photon field encounters gas containing substantial quantities of H_2 , that is, at the edges of dense clouds or Photon Dominated Regions (PDRs). Since our sightlines contain a mix of clouds and H I gas, we might expect just what we apparently are seeing: F I is dominant over HF, but there still may be a bit of HF. For now, the abundance of HF in our observed sightlines is unknown, but apparently less than F I.

Another diatomic species, CF^+ , could be strongly present, but always less so than HF (Neufeld, Wolfire, and Schilke, 2005). From mm-wave emission measurements of the Orion Bar, Neufeld et al. (2006) report $N_{\text{CF}^+} \approx 10^{10}$, whereas the far-UV data from Snow and York (1981), Federman et al. (2005), and this study show that atomic fluorine is three orders

of magnitude larger. The relative abundances of HF and CF⁺ are consistent with the models of Neufeld et al. (2005, 2006), but apparently not the relative abundances of HF and F I.

Regarding depletion onto grains, both Snow and York (1981) and Federman et al. (2005) have discussed this. Snow and York, in the absence of any information on the condensation temperature of fluorine, would have attributed the modest depletion to the high ionization potential (I.P.) of fluorine, following Snow (1975), who found an inverse correlation between I.P. and depletion. Recently, however, a condensation temperature was published by Lodders (2003), who gives a value for fluorine of about 730 K. This should lead to substantial (on order of 0.8 to 1.0 dex) depletion if fluorine followed a correlation with condensation temperature (see review by Savage and Sembach 1996). Neufeld et al. (2005) infer in their models a depletion of 1.7 dex. On the other hand, if the inverse correlation with I.P. holds, then with an I.P. of 17.422 eV, fluorine should be undepleted, more closely approximating what we see.

It is not clear why fluorine is not bound onto the grains. Fluorine is such a rare element that models of dust grains, extinction, and grain surface reactions usually ignore it. But given the reactivity of atomic fluorine with molecular hydrogen, and given that interstellar grains are presumed to be coated with H₂, it would be seem that HF and other fluorine compounds should form on grains and that therefore a significant fraction of the extant fluorine should reside there. This, along with the gas-phase chemistry analyzed by Neufeld et al. (2005, 2006), combined with the detections of HF and CF⁺ in PDRs, makes it likely that most of fluorine is in molecular form in dark clouds, as predicted. But until the most likely molecular species, such as HF and CH⁺, are detected in the same diffuse molecular lines of sight where F I is also observed, we remain unsure of the dominant state of fluorine in those regions.

This research was supported by FUSE grant NNG05GA85G and COS grant NAS5-98043. We are grateful for several useful and stimulating comments made by the anonymous referee. We would also like to thank Rachel Wiley for her assistance in editing this publication.

REFERENCES

- Anders, E., & Grevesse, N. 1989, *GeCoA*, 53, 197.
- Asplund, M., Grevesse, N., & Sauval, A. J. 2005, *ASPC*, 336, 25.
- Cartledge, Stefan I. B., Lauroesch, J. T., Meyer, David M., & Sofia, U. J. 2004, *ApJ*, 613, 1037.

- Cunha, K., Smith, V. V., Lambert, D. L., & Hinkle, K. H. 2003, *AJ*, 126, 1305.
- Diplas, A., & Savage, B. D. 1994, *ApJS*, 93, 211.
- Federman, S. R., Sheffer, Yaron, Lambert, David L., & Smith, V. V. 2005, *ApJ*, 619, 884.
- Forestini, M., Goriely, S., Jorissen, A., & Arnould, M. 1992, *A&A*, 261, 157.
- Jenkins, E. B., & Tripp, T. M. 2001, *ApJS*, 137, 297.
- Jensen, A. G., Rachford, B. L., & Snow, T. P. 2006, *ApJ*, Submitted
- Jorissen, A., Smith, V. V., & Lambert, D. L. 1992, *A&A*, 261, 164.
- Lodders, K. 2003, *ApJ*, 591, 1220.
- Meynet, G., & Arnould, M. 2000, *A&A*, 355, 176.
- Neufeld, D. A. et al. 2006, *A&A*, 454, 37
- Neufeld, D. A., Wolfire, M. G., & Schilke P. 2005, *ApJ*, 628, 260.
- Neufeld, D. A., Zmuidzinas, J., Schilke, P., & Phillips, T. G. 1997, *ApJ*, 488, 141
- Rachford, B. L., et al. 2002, *ApJ*, 577, 221.
- Renda, A., et al. 2005, *NuPhA*, 758, 324
- Savage, B. D., & Sembach, K. R. 1996, *ARA&A*, 34, 279
- Snow, T. P., Jr. 1975, *ApJ*, 202, 87
- Snow, T. P., & McCall, B. J. 2006, *ARA&A*, 44, 367
- Snow, T. P., & York, D. G. 1981, *ApJ*, 247, L39.
- Werner, K., Rauch, T., & Kruk, J. W. 2005, *A&A*, 433, 641.
- Woosley, S. E., & Haxton, W. C. 1988, *Nature*, 334, 45.
- Woosley, S. E., & Weaver, Thomas A. 1995, *ApJS*, 101, 181.
- Zhang, Y., & Liu, X.-W. 2005, *ApJ*, 631, L61.
- Zhu, C., Kreams, R., Dalgarno, A., & Balakrishnan, N. 2002, *ApJ*, 577, 795.

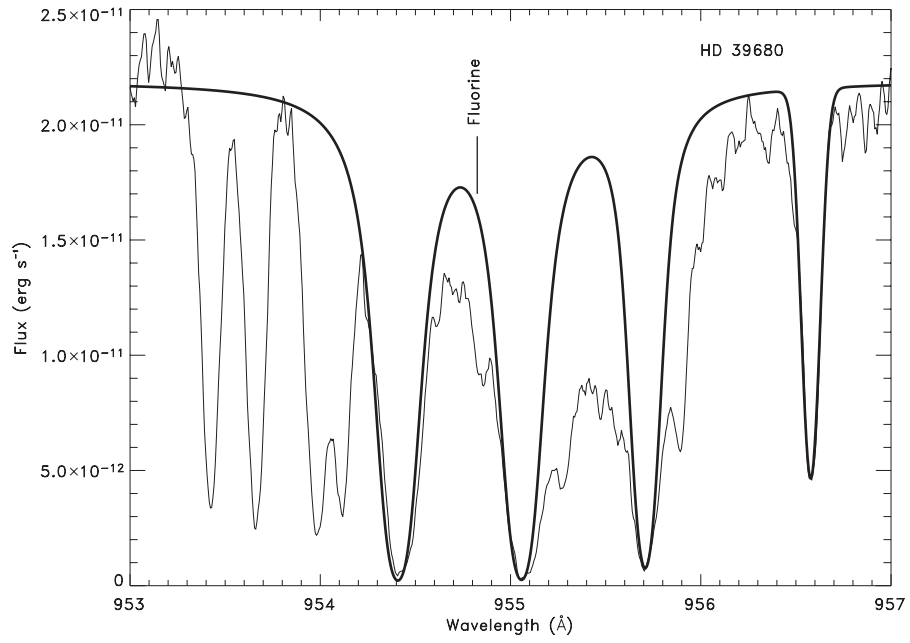


Fig. 1.— Stellar spectrum for HD 39680 in the region around the 954 Å F I line with the derived H_2 model overlaid (bold).

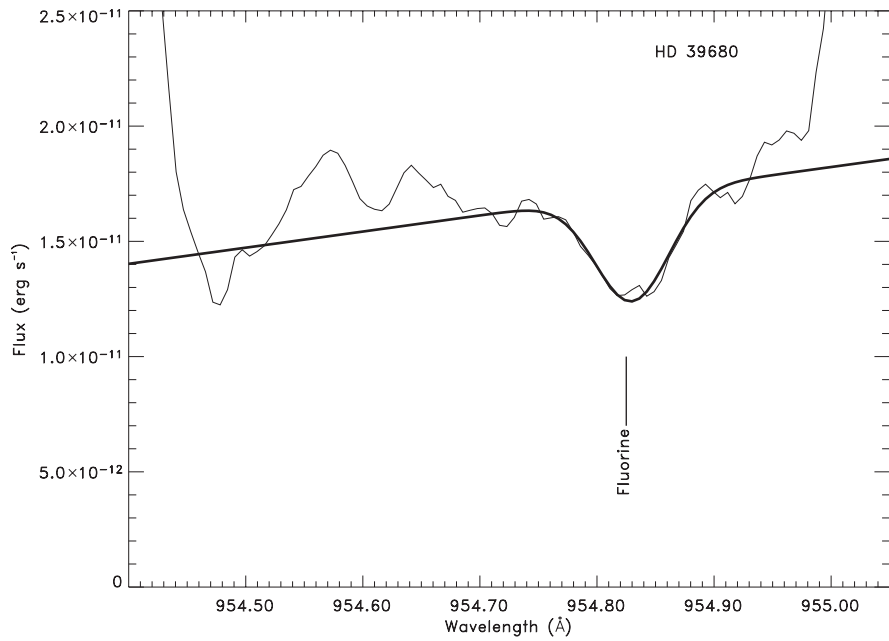


Fig. 2.— Fitting of 954 Å F I line with a single Gaussian after dividing out the H_2 for HD 39680.

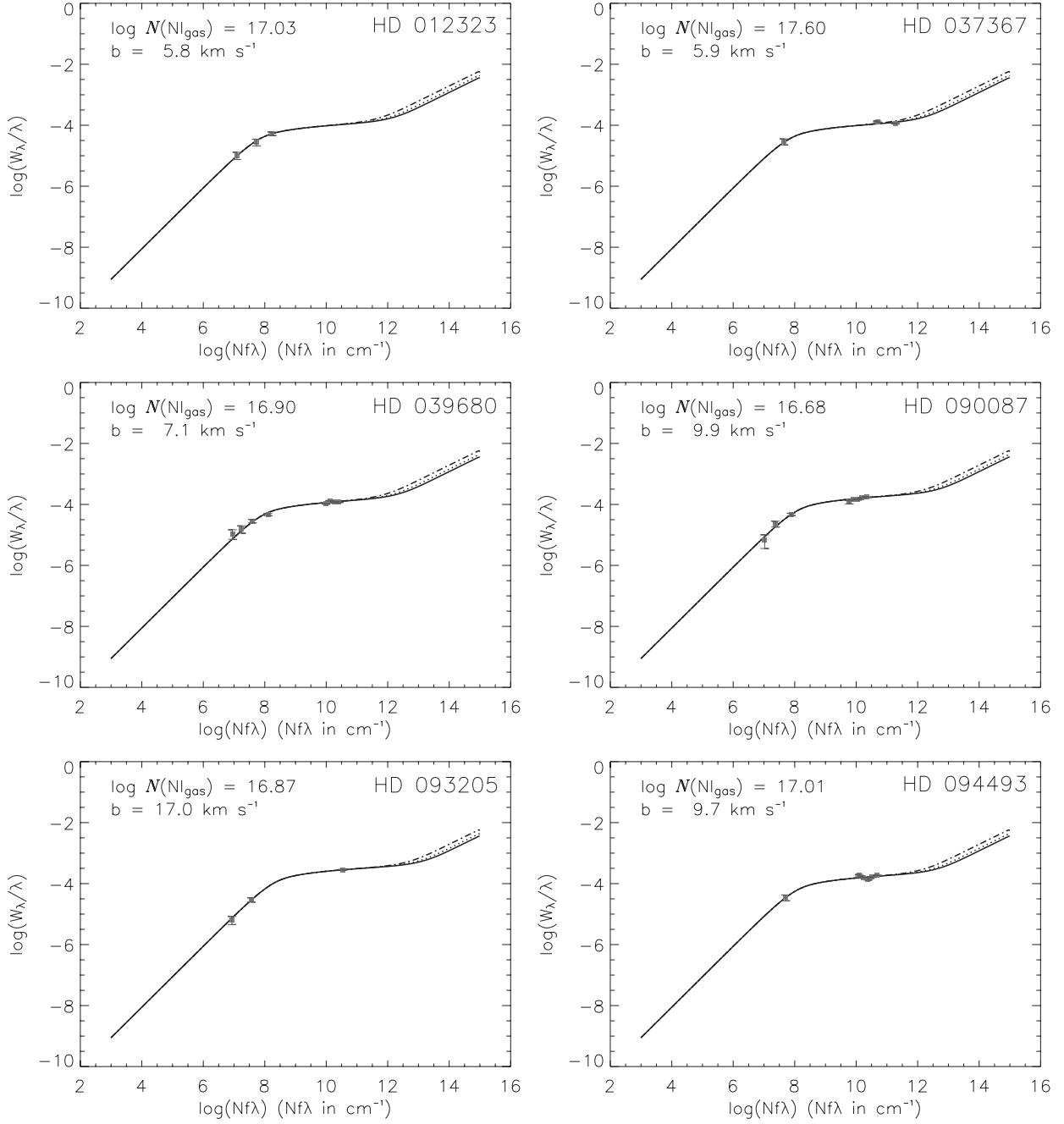


Fig. 3.— N I curves of growth for HD 12323 through HD 94493. Measured equivalent widths and error bars are plotted on top of the appropriate curve for the derived column density and b -value. The solid, dotted, and dotted-dashed lines in the damping portion of the curve represent damping constants of 1.51×10^8 , 2.19×10^8 , and 4.07×10^8 , respectively.

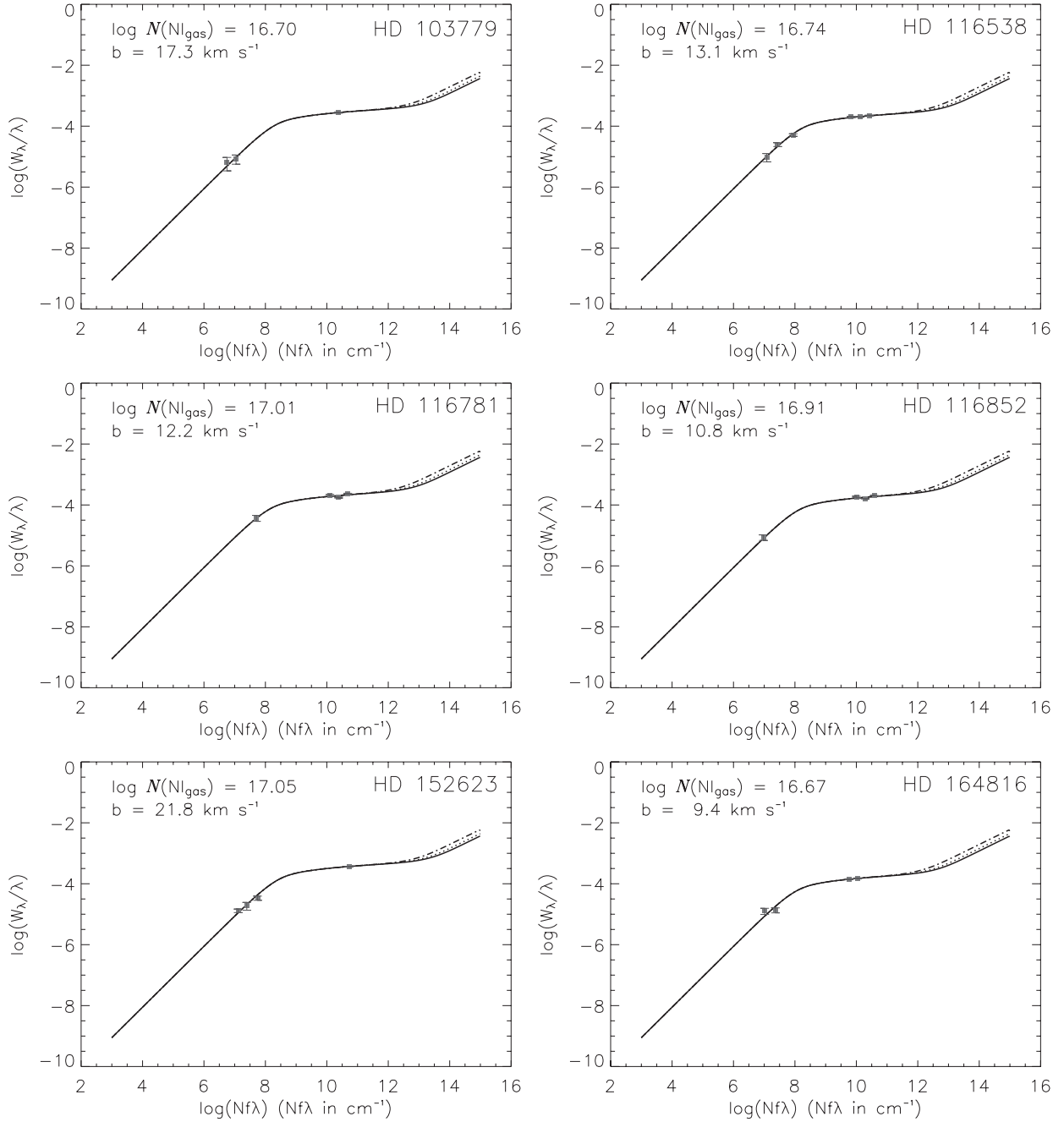


Fig. 4.— N I curves of growth for HD 103779 through HD 164816. Symbols and curves are the same as those in Figure 3.

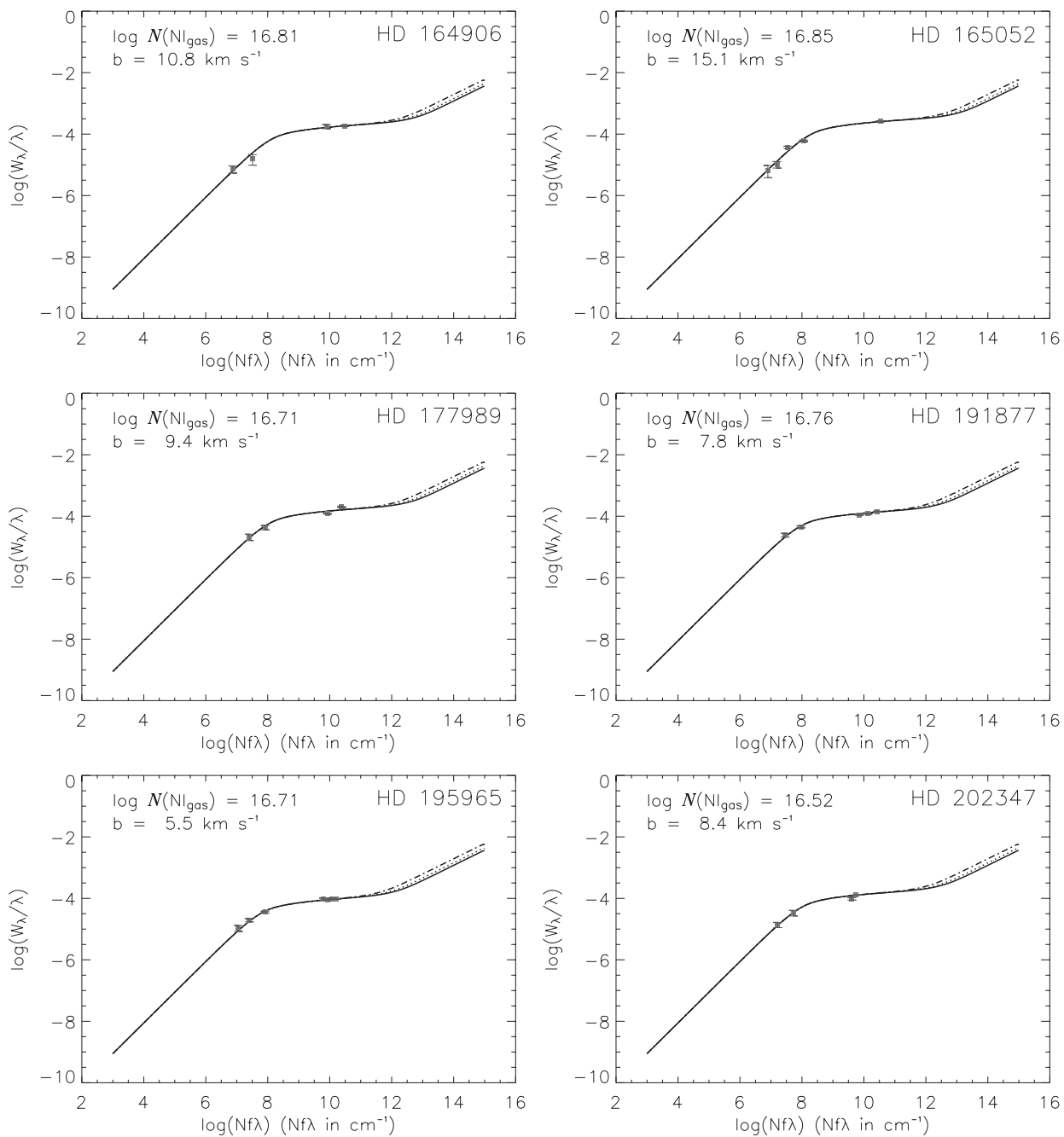


Fig. 5.— N I curves of growth for HD 164906 through HD 202347. Symbols and curves are the same as those in Figure 3.

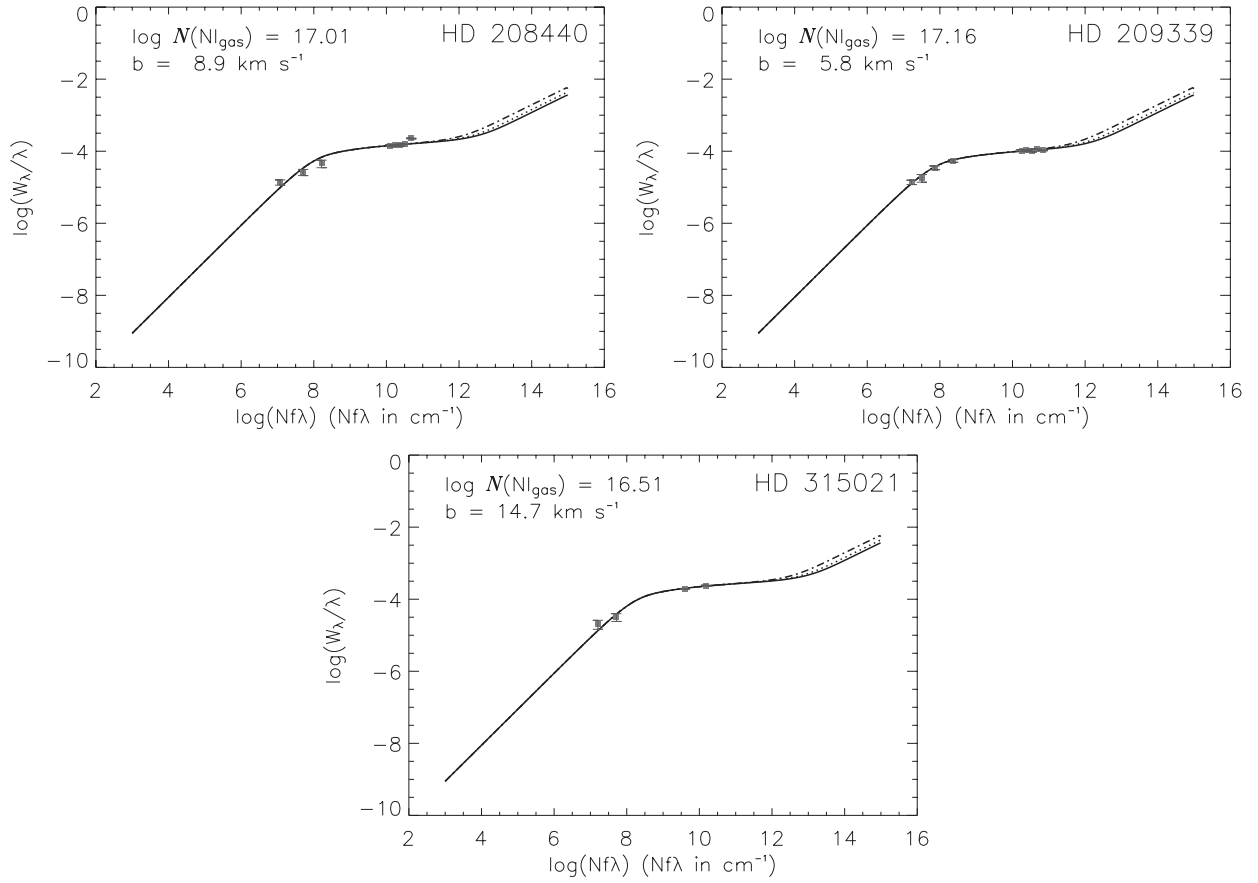


Fig. 6.— N I curves of growth for HD 208440, HD 209339, and HD 315021. Symbols and curves are the same as those in Figure 3.

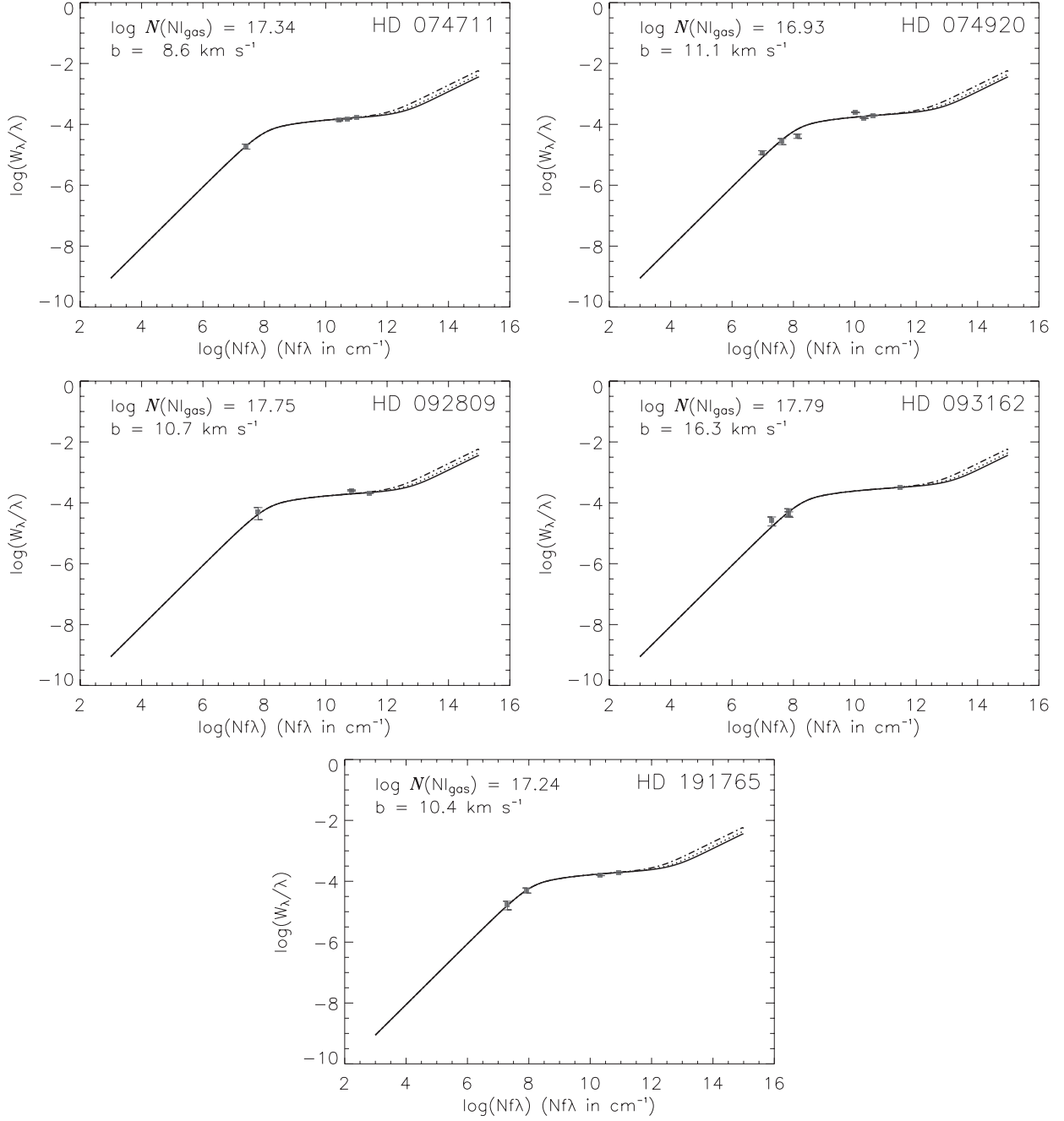


Fig. 7.— N I curves of growth for lines of sight through supernova remnants and to Wolf-Rayet stars. Symbols and curves are the same as those in Figure 3.

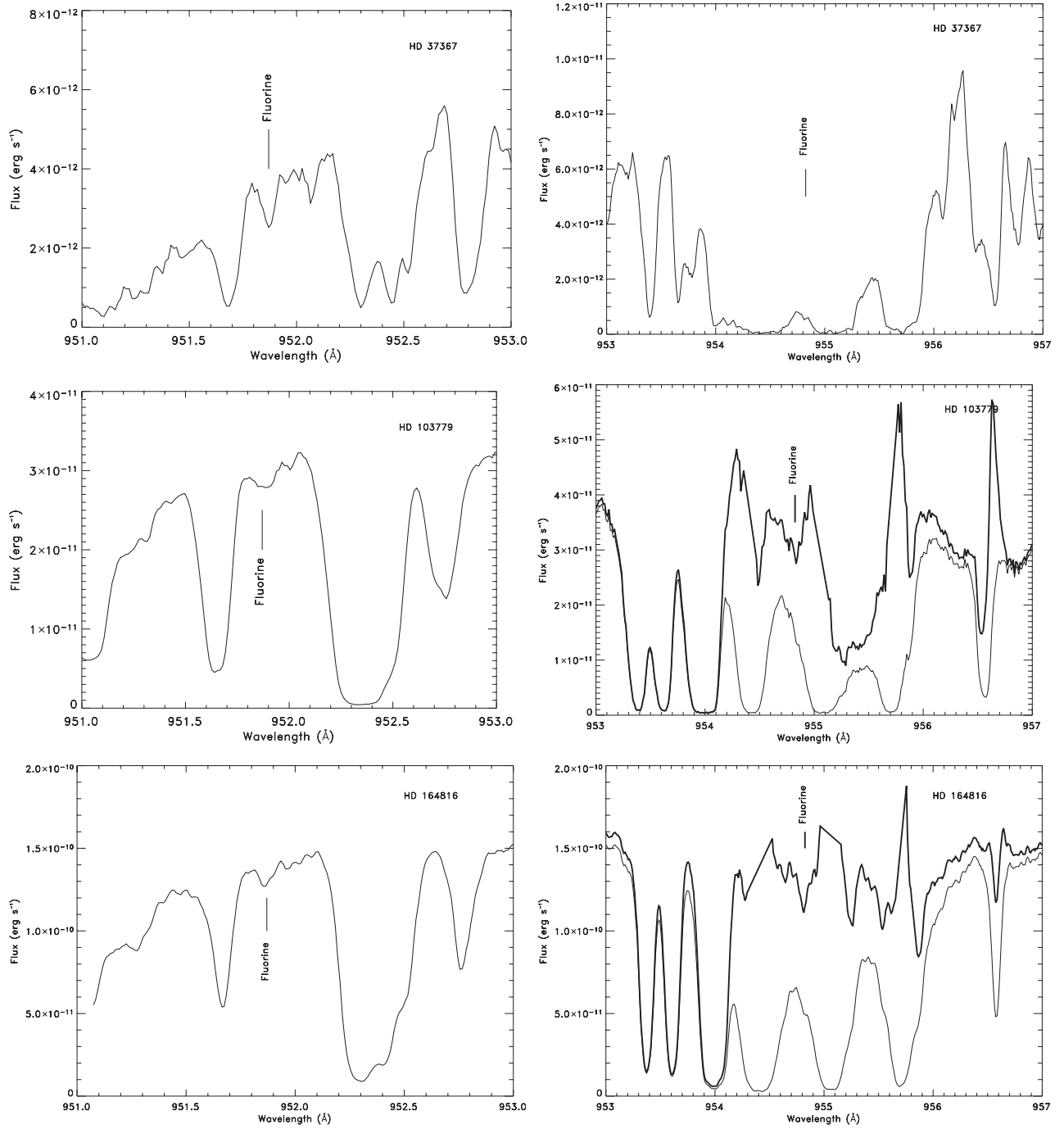


Fig. 8.— Regions surrounding the 951 Å (left) and 954 Å (right) FI lines for HD 37367 (top), HD 103779 (middle), and HD 164816 (bottom). Both the original spectra and the spectra after the H_2 was divided out (in bold) are shown in the 954 Å case for HD 103779, and HD 164816.

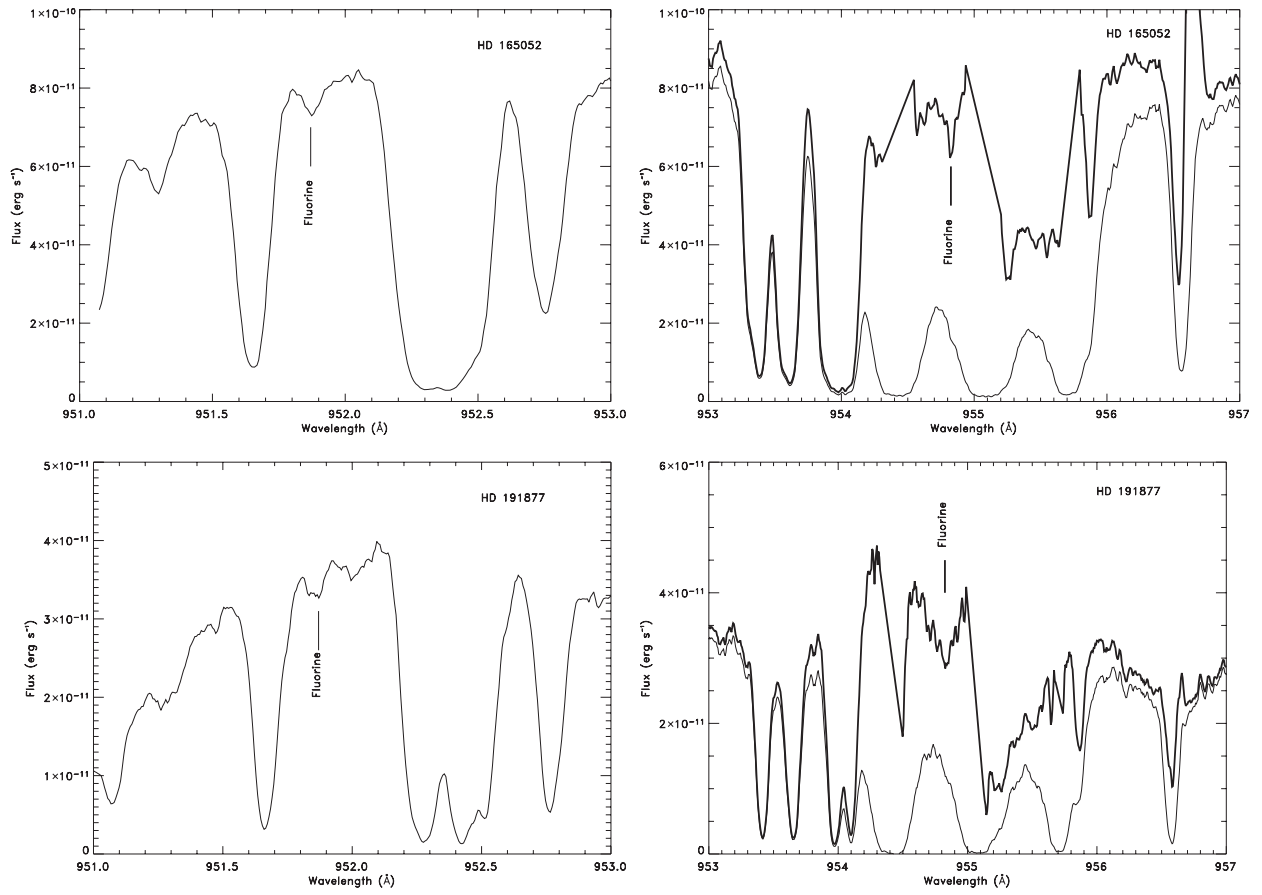


Fig. 9.— Same as Figure 8 but for HD 165052 (top) and HD 191877 (bottom).

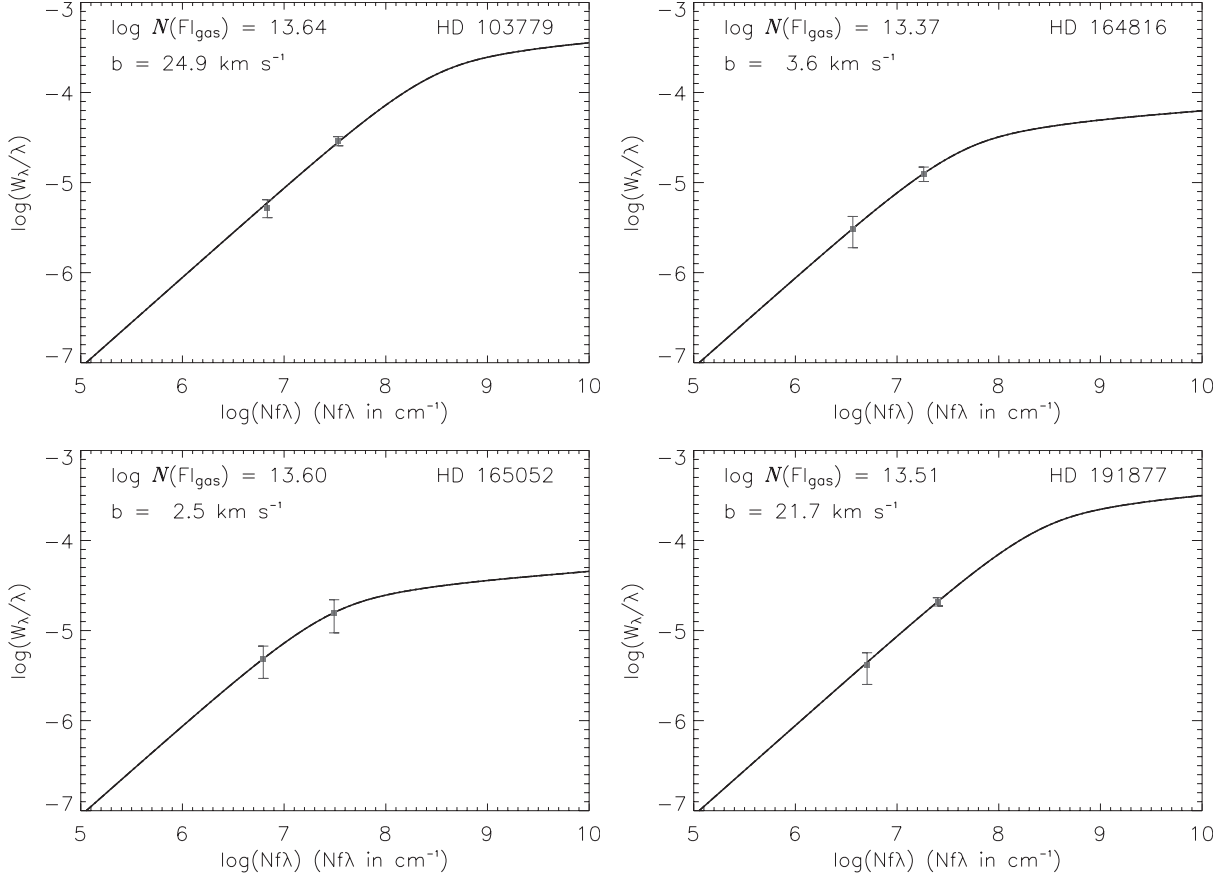


Fig. 10.— F I curves of growth for lines of sight where both F I lines were measured. Measured equivalent widths and error bars are plotted on top of the appropriate curve for the derived column density and b -value. In all cases we observe the ratio of F I equivalent widths to be consistent with little to no saturation. This low level of saturation is also predicted by the N I curve of growth.

Table 1. Stellar Data

Star (HD)	Type	E(B-V)	V	Distance (kpc)	N_{HI}	$N_{H_2}^d$	N_H	Molecular Frac
12323	B9	0.29	8.92	2.29	21.18 ^c	20.31	21.28	0.21
37367	B2IV	0.40	5.99	0.36	21.28 ^c	20.62	21.44	0.30
39680	O6:pe	0.34	7.89	2.48	21.30 ^a	19.53	21.31	0.03
90087	B2/B3III	0.28	7.80	2.72	21.15 ^a	19.91	21.17	0.10
93205	O3V	0.37	7.76	2.63	21.33 ^a	19.79	21.34	0.06
94493	B0.5Iab/Ib	0.20	7.27	3.33	21.11 ^a	20.12	21.15	0.17
103779	B0.5II	0.21	7.22	4.07	21.16 ^a	19.83	21.20	0.09
116538	B2Ib/II	0.17	7.88	1.11	21.04 ^a	19.63	21.06	0.07
116781	B0:Iab:e	0.43	7.45	1.49	21.18 ^b	20.06	21.24	0.13
116852	O9III	0.22	8.49	4.80	20.96 ^a	19.78	20.99	0.12
152623	O8	0.44	6.68	1.91	21.28 ^a	20.21	21.32	0.15
164816	O+	0.31	7.09	1.59	21.18 ^a	20.00	21.21	0.12
164906	O+	0.42	7.45	1.59		20.22		-
165052	A5	0.41	7.76	1.59	21.36 ^a	20.20	21.42	0.12
177989 ^e	B0III	0.25	9.34	4.91	20.95 ^a	20.12	21.06	0.23
191877	B1Ibe	0.18	6.27	2.22	20.89 ^a	20.02	20.95	0.21
195965	B0V	0.25	6.98	0.79	20.90 ^a	20.36	21.01	0.37
202347	B1V	0.17	7.50		20.99 ^b	19.98	21.07	0.16
208440	B1V	0.34	7.91	0.62	21.23 ^a	20.29	21.28	0.19
209339	B0IV		6.69	0.85	21.16 ^b	20.21	21.25	0.18
315021	B3V	0.31	8.59	1.59	21.28 ^a	19.99	21.32	0.09
Wolf-Rayet Stars								
92809	WC6	0.22	9.08			20.23		-
93162	WN+	0.62	8.11	2.60	21.55 ^a	19.83	20.56	0.19
191765	WN6	0.45	8.31		21.48 ^a	20.27	21.51	0.06
Stars Behind Supernova Remnants								
74711	B1III	0.33	7.11			20.30		-
74920	O+	0.34	7.54	1.50	21.15 ^a	20.26	21.20	0.21

^aH I data taken from Diplaz & Savage (1994).

^bH I data taken from Jensen et al. (in preparation).

^cH I data taken from Cartledge et al. (2004).

^d H_2 data were taken from Shull et al. (in preparation).

^eHD 177989 lies behind the Scutum Supershell.

Table 2. New H₂ Column Densities

Star (HD)	$N_{J=0}$	$N_{J=1}$	$N_{J=2}$
37367	20.36 ± 0.04	20.29 ± 0.07	18.64 ± 0.25
74711	20.08 ± 0.05	19.97 ± 0.07	18.32 ± 0.15
92809	19.88 ± 0.06	19.94 ± 0.05	18.87 ± 0.10
93162	19.40 ± 0.03	19.68 ± 0.04	18.54 ± 0.11
94493	19.85 ± 0.06	19.78 ± 0.02	18.55 ± 0.17
116538	19.24 ± 0.05	19.44 ± 0.02	18.30 ± 0.16
164906	19.96 ± 0.02	19.88 ± 0.02	17.95 ± 0.25
191765	19.91 ± 0.11	19.95 ± 0.12	18.76 ± 0.13
202347	19.66 ± 0.05	19.72 ± 0.06	18.26 ± 0.16
208440	20.04 ± 0.05	19.96 ± 0.02	18.39 ± 0.06
209339	19.83 ± 0.03	19.96 ± 0.04	17.79 ± 0.16
315021	19.57 ± 0.03	19.78 ± 0.02	18.08 ± 0.16

Table 3. F I W_λ

Star (HD)	$F_{954} W_\lambda$ (mÅ)	$F_{951} W_\lambda$ (mÅ)
12323	$\leq 59^a$	$\leq 20^a$
37367	$\leq 78^a$	20 ± 7
39680	20 ± 4	$\leq 11^a$
90087	15 ± 3	$\leq 6^a$
93205	$\leq 30^a$	$\leq 8^a$
94493	20 ± 8	$\leq 13^a$
103779	21 ± 3	5.0 ± 1.1
116538	8 ± 4	$\leq 6^a$
116781	$\leq 17^a$	$\leq 10^a$
116852	$\leq 10^a$	$\leq 7^a$
152623	$\leq 27^a$	$\leq 14^a$
164816	12 ± 2	2.9 ± 1.1
164906	$\leq 55^a$	$\leq 17^a$
165052	15 ± 6	4.6 ± 1.8
177989	18 ± 7	$\leq 9^a$
191877	20 ± 2	3.9 ± 1.5
195965	$\leq 23^a$	$\leq 3^a$
202347	7 ± 3	$\leq 6^a$
208440	19 ± 7	$\leq 15^a$
209339	16 ± 6	$\leq 13^a$
315021	18 ± 5	$\leq 6^a$
Wolf-Rayet Stars		
92809	$\leq 37^a$	$\leq 36^a$
93162	$\leq 30^a$	$\leq 27^a$
191765	$\leq 44^a$	$\leq 22^a$
Supernova Remnants		
74711	$\leq 30^a$	$\leq 24^a$
74920	$\leq 58^a$	$\leq 11^a$

^aTwo sigma upper limit

Table 4. Interstellar N I Column Densities and b -values

Star (HD)	N_{NI}	b -value (km s ⁻¹)
12323	17.03	5.8
37367	17.60	5.9
39680	16.90	7.1
90087	16.68	9.9
93205	16.87	17.0
94493	17.01	9.7
103779	16.70	17.3
116538	16.74	13.1
116781	17.01	12.2
116852	16.91	10.8
152623	17.05	21.8
164816	16.67	9.4
164906	16.81	10.8
165052	16.85	15.1
177989	16.71	9.4
191877	16.76	7.8
195965	16.71	5.5
202347	16.52	8.4
208440	17.01	8.9
209339	17.16	5.8
315021	16.51	14.7
Wolf-Rayet Stars		
92809	17.75	10.7
93162	17.79	16.3
191765	17.24	10.4
Supernova Remnants		
74711	17.34	8.6
74920	16.93	11.1

Table 5. Interstellar F I Column Densities and Depletions

Star (HD)	N_F	Depletion ^b
12323	$\leq 14.57^a$	$\leq +0.73^a$
37367	$14.32_{-0.24}^{0.19}$ ^c	$+0.32^c$
39680	$13.58_{-0.12}^{0.09}$	-0.29
90087	$13.39_{-0.13}^{0.10}$	-0.34
93205	$\leq 13.71^a$	$\leq -0.19^a$
94493	$13.55_{-0.25}^{0.17}$	-0.16
103779	$13.53_{-0.05}^{0.06}$	-0.23
116538	$13.10_{-0.30}^{0.18}$	-0.52
116781	$\leq 13.46^a$	$\leq -0.34^a$
116852	$\leq 13.21^a$	$\leq -0.34^a$
152623	$\leq 13.65^a$	$\leq -0.23^a$
164816	$13.29_{-0.08}^{0.08}$	-0.48
164906	$\leq 14.11^a$	-
165052	$13.39_{-0.23}^{0.15}$	-0.59
177989	$13.49_{-0.23}^{0.17}$	-0.13
191877	$13.57_{-0.06}^{0.04}$	0.08
195965	$\leq 13.69^a$	$\leq 0.12^a$
202347	$13.05_{-0.25}^{0.16}$	-0.58
208440	$13.52_{-0.21}^{0.17}$	-0.32
209339	$13.47_{-0.23}^{0.18}$	-0.34
315021	$13.47_{-0.14}^{0.12}$	-0.41
Wolf-Rayet Stars		
92809	$\leq 13.86^a$	-
93162	$\leq 13.71^a$	$\leq 0.59^a$
191765	$\leq 13.97^a$	$\leq -0.10^a$
Supernova Remnants		
74711	$\leq 13.77^a$	-
74920	$\leq 14.14^a$	$\leq +0.38^a$

^aTwo sigma upper limit

^bDepletions are based on the solar value $F/H = 3.63 \times 10^{-8}$.

^cValues based on the 951 Å F I line.
This F I detection is uncertain due to
potential interference from stellar fea-
tures.

Table 6. Comparison With Previous Work

Star (HD)	N_F (<i>This Study</i>)	N_F (<i>Federman</i>)
208440	$13.52^{+0.17}_{-0.21}$	$13.52^{+0.16}_{-0.26}$
209339	$13.47^{+0.18}_{-0.23}$	$13.46^{+0.17}_{-0.28}$

Table 7. Comparison of Methods used to Derive N_F

Star (HD)	N_F		b -value (km s ⁻¹)	
	N I	F I	N I	F I
103779	$13.67^{+0.05}_{-0.05}$	$13.64^{+0.04}_{-0.04}$	17.3	24^{+0}_{-13}
164816	$13.29^{+0.08}_{-0.08}$	$13.37^{+0.10}_{-0.09}$	9.6	3^{+16}_{-3}
165052	$13.39^{+0.15}_{-0.23}$	$13.60^{+0.22}_{-0.19}$	15.1	2^{+22}_{-1}
191877	$13.57^{+0.04}_{-0.06}$	$13.51^{+0.04}_{-0.05}$	7.8	21^{+3}_{-14}

Table 8. Observed lines of sight to Wolf-Rayet stars or through supernova remnants

Star (HD)	Problem with line of sight
Wolf-Rayet Stars	
32402	Interference from other absorption features
33133	Noise and insufficient flux in 954 Å region
37026	Interference from other absorption features
37680	Interference from other absorption features
96548	Insufficient flux in 954 Å region
104994	Noise and insufficient flux in 954 Å region
151932	Insufficient flux in 954 Å region
164270	Insufficient flux in 954 Å region
187282	Interference from other absorption features
192163	Insufficient flux in 954 Å region
192641	Noise and insufficient flux in 954 Å region
269582	Noise and insufficient flux in 954 Å region
Supernova Remnants	
5980	Interference from other absorption features
36665	Insufficient flux in 954 Å region
37318	Insufficient flux in 954 Å region
47240	High velocity components interfere with 951 Å region
72088	Noise and insufficient flux in 954 Å region
72350	Noise and insufficient flux in 954 Å region